Assessment of a Common Non-Linear Eddy-Viscosity Turbulence Model in Capturing Laminarization in Mixed Convection Flows

Amir Keshmiri[1,2,*], Alistair Revell[2] and Hamidreza Gohari Darabkhani[3]

[1]*School of Engineering, Manchester Metropolitan University, Manchester, M1 5GD, U.K.*

[2]*School of Mechanical, Aerospace and Civil Engineering (MACE), The University of Manchester, Manchester, M13 9PL, U.K.*

[3]*Institute for Energy and Resource Technology (IERT), School of Applied Sciences, Cranfield University, Cranfield, MK43 0AL, U.K.*

[*] *Corresponding author: email: a.keshmiri@mmu.ac.uk; Tel:+44(0)161 2471695.*

Short Title: Assessment of Suga NLEVM in Mixed Convection

ABSTRACT

Laminarization is an important topic in heat transfer and turbulence modelling. Recent studies have demonstrated that several well-known turbulence models, failed to provide accurate prediction when applied to mixed convection flows with significant re-laminarization effects. One of those models, a well-validated cubic non-linear eddy-viscosity model, was observed to miss entirely this feature. This paper studies the reasons behind this failure by providing a detailed comparison with the baseline Launder-Sharma model. The difference is attributed to the method of near-wall damping. A range of tests have been conducted and two noteworthy findings are reported for the case of flow re-laminarization.

Keywords: Turbulence Modelling, Mixed Convection, Laminarization, Non-Linear Eddy-Viscosity Models, Heat Transfer, Thermal-Hydraulics.

NOMENCLATURE

Bo = Buoyancy parameter, $8\times10^4\, Gr/(Re^{3.425}Pr^{0.8})$

c_f = Local friction coefficient

C_μ = Constant in Eddy-Viscosity Models

D = Pipe diameter

E_ε = Near-wall source term

f_μ = Damping function

g_i = Acceleration due to gravity

Gr = Grashof number, $\beta g D^4 \dot{q} / (\lambda \nu^2)$

k = Turbulent kinetic energy, $\overline{u_i u_i} / 2$

Nu = Nusselt number, $\dot{q} D / \lambda (T_w - T_b)$

p = Pressure

P_k = Rate of shear-production of k, $-\overline{u_i u_j} \left(\partial U_i / \partial x_j \right)$

Pr = Prandtl number, $c_p \mu / \lambda$

$\dot{q}$ = Wall heat flux

R = Pipe radius

Re = Reynolds number, $U_b D / \nu$

Re_t = Turbulent Reynolds number, $k^2 / (\nu \tilde{\varepsilon})$

S = Strain parameter

T = Temperature

T^+ = Non-dimensional temperature, $(T_w\text{-}T)/T_\tau$

T_τ = Friction temperature, $\dot{q}/\rho.c_p.U_\tau$

U^+ = Non-dimensional velocity, U/U_τ

U_τ = Friction velocity, $(\tau_w / \rho)^{1/2}$

U_i, u_i = Mean, fluctuating velocity components in Cartesian tensors

$\overline{u_i u_j}$ = Reynolds stress tensor

$\overline{u_i \theta}$ = Turbulent heat flux

x, y = Streamwise and wall-normal coordinates

y^+ = Dimensionless distance from the wall, $y U_\tau / \nu$

Greek Symbols:

β = Coefficient of volumetric expansion

δ_{ij} = Kronecker delta

ε = Rate of dissipation of k

λ = Thermal conductivity

μ = Dynamic viscosity

ν = Kinematic viscosity, μ / ρ

ν_t = Turbulent viscosity

ρ = Density

σ_t = Turbulent Prandtl number

τ_w = Wall shear stress

Subscripts:

0 = Forced Convection

b = Bulk

t = Turbulent

w = Wall

Acronyms:

CFD = Computational Fluid Dynamics

DNS = Direct Numerical Simulations

EVM = Eddy-Viscosity Models

LEVM = Linear Eddy-Viscosity Models

LS = Launder-Sharma Model

NLEVM = Non-Linear Eddy-Viscosity Models

RANS = Reynolds-Averaged Navier-Stokes

TKE = Turbulent Kinetic Energy

TVR = Turbulent Viscosity Ratio

Additional symbols are defined in the text.

1 INTRODUCTION

Conduction, convection and radiation are the three modes of heat transfer. Convection is said to occur when there is a transport of thermal energy by molecular conduction and bulk fluid motion and it is traditionally divided into ‘forced’ and ‘natural’ convection. However, forced and natural convection may exist simultaneously when there is a buoyancy-modified forced flow and the heat transfer regime is termed ‘mixed’ convection. The effects on heat transfer performance are complex, and their effects do not combine in a simple additive manner. The complexities of mixed convection are mainly associated with the behaviour of fluid flow in the near-wall region.

In laminar mixed convection, the near-wall velocity is increased in ascending (i.e. buoyancy-aided) flows and decreased in descending (i.e. buoyancy-opposed) flows, consequently, heat transfer is enhanced and impaired, respectively. In turbulent flows, however, the impairment or enhancement of the rate of heat transfer is determined by the interaction between the velocity field and the rate of turbulence production in the near-wall region; in the case of descending flow, heat transfer levels are always enhanced, while in the ascending flow case, heat transfer levels may be either impaired (at moderate heat loadings), or enhanced (at very high heat loadings). In ascending mixed convection turbulent flows, by increasing the heat loading,

the advection in the near-wall region is increased, while the turbulence production is reduced due to the decreased level of shear stress in the same region. The net result of this is an impairment of the wall heat transfer, followed by a complete condition of 'laminarization'. The laminarization (which will be further discussed in conjunction with Figure 1) occurs when the shear stress in the near-wall region falls as the result of increased buoyancy force. Following the laminarization phase, any further increase of heat loading would increase the rate of turbulence production and results in heat transfer recovery and enhancement.

'Laminarization' (or 're-laminarization') is an important topic in heat transfer and turbulence modelling [1] and is relevant to a wide range of applications. The test case considered in the present study is related to the post-trip decay heat removal in nuclear reactor cores. The primary focus of this paper is on ascending mixed convection flows which represent the coolant flow in the fuel elements of the UK fleet of 'Advanced Gas-cooled Reactors' (AGRs) [2]. The review papers of Jackson et al. [3] and Jackson [4] provide extended discussions of heat transfer performance under mixed convection conditions. The most popular CFD technique adopted in simulating mixed convection flows have been based on the solution of the Reynolds-Averaged Navier-Stokes (RANS) equations, and amongst the possible turbulence models available to close these equations, the Eddy-Viscosity Models (EVMs) have been employed by the majority of the researchers including Abdelmeguid and Spalding [5], Tanaka et al. [6], Cotton and Jackson [7], Mikielewicz et al. [8], Richards et al. [9], Kim et al. [10] and Keshmiri et al. [11-13], amongst others. Keshmiri et al. [11, 12] recently tested a wide range of RANS turbulence models and found that the *k-ω-SST* model [14] and the non-linear eddy-viscosity model (NLEVM) of Craft, Launder and Suga [15] completely failed to capture the laminarization phenomenon present in ascending mixed convection flows. This was a particularly significant finding, since these two models are commonly used in several commercial CFD codes, and are 'recommended' by various industrial best practice guidelines for a wide range of applications [13, 16]. Indeed, contrary to expectation associated with some of the more recent turbulence models tested, it was demonstrated that the original 'low-Reynolds-number' model of Launder and Sharma [17] was, in general, the superior model.

The present research focuses on the NLEVM proposed by Craft, Launder and Suga [15] and aims to investigate the reasons for the failure of this model in a benchmark ascending mixed convection flow. While the test case is indeed simple, it provides an unambiguous assessment of the physics associated with re-laminarization, and thus observations can be expected to be relevant to more complex applications. While some attempts are made to remedy the identified problem, the calibration of an entirely new model is beyond the scope of this study. Herein we aim to provide information for the purpose of a future study in this direction; i.e. the development of a cubic NLEVM for mixed convection flow; which would be of significant benefit to the nuclear industry.

2 CASE DESCRIPTION

The geometry studied here consists of a vertical pipe for which the thermal boundary condition is one of uniform wall heat flux. The working fluid is assumed to be standard air and the Reynolds number based on the pipe diameter is set to Re = 5,300. The Prandtl number of standard air (Pr = 0.71) is used throughout calculations. In addition, all fluid properties are assumed to be constant, and buoyancy is accounted for within the Boussinesq approximation.

In the results reported in this paper, comparison is made with the Direct Numerical Simulation (DNS) data of You et al. [18], who conducted a study of turbulent mixed convection in a vertical uniformly-heated pipe for constant property conditions. In their work, You et al. accounted for buoyancy via the Boussinesq approximation, which is particularly useful for validation studies, since it permits an examination of buoyancy effects in isolation from other variable property phenomena. In computing mixed convection flows, You et al. [18] retained the same Reynolds and Prandtl numbers and varied buoyancy influence via the Grashof number. A total of four simulations were reported, as shown in Table 1, and a brief description of the thermal-hydraulic regime is provided in each case. The mean flow and turbulence profiles presented in 'Section 6' are reported for the four thermal-hydraulic regimes indicated in Table 1. These flow regimes have been chosen by You et al. specifically to correspond to one forced and three distinctive mixed convection cases. From turbulence modelling point of view, Case (C) represents the most challenging thermal-hydraulic regime and is therefore viewed as the most important case in the present study.

3 COMPUTATIONAL CODE AND MESH

The present computations have been performed using an in-house code, known as 'CONVERT' (for Convection in Vertical Tubes). CONVERT was originally developed by Cotton [19] and later extended by a number of researchers; the latest version which is used here is due to Keshmiri et al. [11]. Differential equations are integrated over a control volume and then discretized, following a parabolic time-marching approach similar to the code described in Leschziner [20]. Solution of the algebraic equations is achieved via the Tri-Diagonal Matrix Algorithm (TDMA).

The mesh used for the present CONVERT computations consists of 100 control volumes and the wall-adjacent node is typically located at y^+ = 0.5, never higher than unity. A number of tests with different mesh refinement have been carried out to ensure grid independence prior to obtaining the results reported below. In all cases, the solution is initialised with an isothermal run in which the dynamic field is allowed to develop from approximate initial profiles to a fully developed state. The production runs read the initialised results at the 'location' x = 0 and are typically run for time corresponding to a flow of 50 diameters downstream of x = 0. Interested readers are referred to Cotton [19] and Keshmiri et al. [11] for further details on CONVERT solution sequence.

4 MEAN FLOW EQUATIONS

The mean flow equations are written in the Boussinesq approximation. Adopting Cartesian tensor notation, the equations read as follows:

Continuity:

$$\frac{\partial U_j}{\partial x_j} = 0 \tag{1}$$

Momentum:

$$\frac{DU_i}{Dt} = -\frac{1}{\rho}\frac{\partial p}{\partial x_i} + \frac{\partial}{\partial x_j}\left(\nu \frac{\partial U_i}{\partial x_j} - \overline{u_i u_j}\right) + \left[1 - \beta(T - T_0)\right] g_i \tag{2}$$

Energy:

$$\frac{DT}{Dt} = \frac{\partial}{\partial x_j}\left[\left(\frac{\nu}{Pr}\frac{\partial T}{\partial x_j} - \overline{u_j \theta}\right)\right] \tag{3}$$

where g_i = [-g, 0, 0] in ascending flow, $\overline{u_i u_j}$ represents the Reynolds stress tensor and $\overline{u_j \theta}$ the turbulent heat flux. In the present computations the turbulent heat fluxes are modelled using the simple eddy-diffusivity approximation, modelled as

$$\overline{u_i \theta} = -\frac{\nu_t}{\sigma_t}\frac{\partial T}{\partial x_i} \tag{4}$$

Following standard modelling practice, the turbulent Prandtl number is set to a constant value, σ_t = 0.9.

5 THE TURBULENCE MODELS

As mentioned above, computations in the present work are conducted using two low-Reynolds number eddy-viscosity-based models, namely the baseline *k-ε* model due to Launder-Sharma (LS) [17] and the non-linear *k-ε* model proposed by Craft, Launder and Suga [15]. Non-linear eddy viscosity models are, perhaps unsurprisingly, intended to offer a greater level of physical realism than the linear *k-ε* model, particularly for the complex geometries one is likely to be faced with in industry [1]. While reported in its full form by Craft et al. [15] this model was originally developed by Suga [21], and is thus here referred to as the 'Suga' model. This model was popularised via its implementation in various commercial CFD software and should improve prediction of the turbulence stress anisotropy via the incorporation of additional terms in the constitutive equation, both quadratic and cubic in mean strain and vorticity. This is particularly significant close to a wall where stress anisotropy is high. Both models were implemented into CONVERT and

validated with results from Suga [21] for a channel flow at Re = 5,600 and 14,000 (based on the DNS data of Kim et al. [22]). The results of these verification and validation tests can be found in [13, 23].

For clarity, the full form of both the LS and the Suga models are reviewed in this section. Both employ the same transport equations for the turbulence kinetic energy and dissipation rate, as indicated below:

$$\frac{Dk}{Dt} = P_k + \frac{\partial}{\partial x_j}\left[\left(\nu + \frac{\nu_t}{\sigma_k}\right)\frac{\partial k}{\partial x_j}\right] - (\tilde{\varepsilon} + D)$$

$$\frac{D\tilde{\varepsilon}}{Dt} = C_{\varepsilon 1}\frac{\tilde{\varepsilon}}{k}P_k + \frac{\partial}{\partial x_j}\left[\left(\nu + \frac{\nu_t}{\sigma_\varepsilon}\right)\frac{\partial \tilde{\varepsilon}}{\partial x_j}\right] - C_{\varepsilon 2} f_\varepsilon \frac{\tilde{\varepsilon}^2}{k} + E_\varepsilon + Y \qquad (5)$$

$$P_k = -\overline{u_i u_j}\left(\partial U_i / \partial x_j\right) \qquad \nu_t = C_\mu f_\mu \frac{k^2}{\varepsilon} \qquad Re_t = k^2 / \nu\tilde{\varepsilon}$$

Given the focus of this paper, it is interesting to examine all points where these two models differ, and a full list of such is provided in Table 2. The model constants are the same for each model where the same constants exist (see Tables 3 and 4).

Note that both models solve for the homogenous dissipation rate, $\tilde{\varepsilon}$, instead of ε. This removes the need for an imposed finite value for the turbulence dissipation rate at the wall and thus increases stability of the model. The substitution is straightforward, since outside the viscous sub-layer $\tilde{\varepsilon} = \varepsilon$, which means all the earlier modelling considerations are still valid, while at the wall, $\tilde{\varepsilon}$ = 0. Also shown in Table 2, the Suga model employs a 'strain-sensitive' C_μ coefficient rather than the constant value C_μ = 0.09, used in the LS model. The proposed expression for C_μ is a function of dimensionless strain and vorticity invariants, which are defined as

$$\tilde{S} = k/\tilde{\varepsilon}\sqrt{1/2(S_{ij}S_{ij})} \quad , \quad \tilde{\Omega} = k/\tilde{\varepsilon}\sqrt{1/2(\Omega_{ij}\Omega_{ij})} \qquad (6)$$

where the mean strain rate and vorticity tensor are

$$S_{ij} = \left(\frac{\partial U_i}{\partial x_j} + \frac{\partial U_j}{\partial x_i}\right) \quad , \quad \Omega_{ij} = \left(\frac{\partial U_i}{\partial x_j} - \frac{\partial U_j}{\partial x_i}\right) \qquad (7)$$

Although this variable form of C_μ is expected to improve the prediction of turbulence in response to non-equilibrium strain rates, it does not imply any normal stress anisotropy. Instead, additional terms are added to the stress-strain relation which approximate the Reynolds stresses via a function of mean velocities and vorticities. Craft et al. [15] optimised the coefficients appearing in the constitutive equation of the Suga model over a range of flows including simple shear, impinging, curved and swirling flows. Their proposed values are listed in Table 4. Another term sometimes included in the ε-equation of the LS and Suga model is the Yap term, (proposed by Yap [24]) which is a length-scale correction term. This correction was

designed to prevent the LS model from returning excessively large length-scales, especially in reattaching and impinging flows, however, it has not been included in the calculations presented in the present paper since Keshmiri [12] has shown that in ascending mixed convection flows, including the Yap term has no effects on heat transfer and friction coefficient. Generally, this correction term becomes active when the predicted turbulent length-scale exceeds the equilibrium length-scale which is not the case in ascending mixed convection flow problems.

Finally, from Table 2 it can be seen that the expression for near-wall source term, E_ε, is different from its original form in the LS model. This term acts to increase the dissipation rate in the near wall region, where velocity gradients are changing rapidly. A new expression for E_ε has been adopted in the Suga model in order to reduce its dependence on the Reynolds number.

6 RESULTS AND DISCUSSION

6.1 Results of Forced Convection

Since forced convection Nusselt number (Nu_0) and friction coefficient (c_{f0}) are to supply the normalising parameter in the presentation of heat transfer and friction coefficient impairment/enhancement effects, it is appropriate first to assess model performance in the computation of buoyancy-free pipe flows. The results of this initial assessment are summarised in Table 5 which compares the values of local Nusselt number and friction coefficient obtained by the Suga and LS models against the DNS data of You et al. [18]. It is noted that the LS model somewhat under-predicts the DNS values of Nu_0 and c_{f0}, while the value of Nu_0 returned by the Suga model is in very good agreement with the DNS data. The prediction of the Suga model for the friction coefficient is also closer to the data compared to the LS model.

6.2 Results of Local Nusselt Number and Friction Coefficient

Figure 1 shows the heat transfer performance for both the Suga and LS models for an ascending flow. The Nusselt number in mixed convection, Nu, is normalised by the corresponding forced convection value evaluated at the same Reynolds and Prandtl numbers, and Nu/Nu_0 is plotted against the buoyancy parameter, Bo. The DNS data of You et al. [18], and the experimental results of Steiner [25], Carr et al. [26] and Parlatan et al. [27] are also included. The most remarkable observation from Figure 1 is the dramatic reduction in heat transfer levels occurring in the interval $0.15 < Bo < 0.25$. We recall that DNS Case (C) ($Bo = 0.18$) is representative of the laminarized state, in which heat transfer levels are around 40% of those found in forced convection, under otherwise identical conditions. It can be seen that the predictions of the LS model formulation is in close agreement with the three DNS data points. The shortcoming of the Suga model is then immediately clear, in that the model appears to be unable to predict the correct level of the heat transfer impairment indicated by the DNS. Furthermore, the onset of this impairment is delayed

significantly. However, in the 'recovery' region ($Bo \geq 0.5$) the Suga model is in reasonable agreement with the data of Steiner [25].

Turning to examine the friction coefficient, Figure 2 displays the normalised local friction coefficient plotted against the buoyancy parameter. Both models indicate little or no reduction in friction coefficient below the c_{f0} level. In the case of the LS model this is, at least in part, related to its under-prediction of c_{f0} by about 8% (Table 5). In turn, this results in an earlier onset of friction coefficient enhancement compared to the experimental results of Carr et al. [26] and DNS data. In comparison to the LS model, the results of the Suga model indicate a steeper enhancement gradient.

In comparing Figure 1 to Figure 2, it is noted that the reduction of friction coefficient due to laminarization is significantly less than that of heat transfer. In addition, c_f/c_{f0} rises to a value greater than unity for Case (C) (Bo = 0.18), while under the same conditions the heat transfer coefficient is much lower than one. These differences lead to a conclusion that in a buoyancy-influenced flow the relationship between momentum transfer and heat transfer is less direct than in forced convection [10].

It is worth noting that in both Figures 1 and 2, there is some scatter in the reference data, particularly the experimental measurements of Parlatan et al. [27]. In their DNS work, You et al. [18] explained that while their results did not agree well with experimental data obtained by imposing the total pressure drop (e.g. Parlatan et al. [27]), they observed closer agreement with those obtained by measurement of velocity gradient instead (e.g. Carr et al. [26]). In addition, discrepancies are likely to arise from different methods of measuring c_f.

6.3 Mean Flow Profiles

Mean flow and turbulent shear stress profiles obtained using both the Suga and LS models are plotted in Figure 3. Focussing first of all on the predictions from the Suga model, it can be seen from Figure 3(a) and (b) that the velocity predictions of the Suga model for the first three cases (Cases A-C) remain essentially unchanged; demonstrating the insensitivity of this model to the laminarization effect. The Suga model is then observed to respond correctly to buoyancy effects at higher Bo numbers, as indicated by the 'M-shape' profile for Case (D). In both velocity and temperature profiles, the maximum discrepancies occur at the pipe centre-line, particularly so for Case (C). Considering now the same analysis for the LS model, a much improved response to the different conditions is observed. Results for Cases (A) and (B) are good, and while those for (C) and (D) exhibit a slight under-prediction of momentum at the centre-line, they are far improved versus the same predictions from the Suga model. It is worth also to note from Figure 3(b) that the mean velocity profiles are plotted in wall coordinates and highlight the departure from near-wall 'universality' (i.e. the log-law) under conditions of turbulent mixed convection. As such, any assumption of universality made in order to construct wall functions for use with 'high-Reynolds-number' turbulence

models applied to mixed convection are clearly questionable, underlining the need for modelling of the viscous sub-layer in these flows [7].

In Figure 3(c), the temperature profiles returned by the LS model are in very good agreement with the DNS data, while the Suga model returns poor results for Cases (C) and (D). When plotting the temperature profiles in wall units (shown as insets in Figure 3c), these discrepancies become more apparent. This is particularly evident from the results of the Suga model, mainly due to an inaccurate estimation of τ_w by the model (see also friction coefficient distributions in Figure 2).

Already the general trend is emerging; that the extra modelling complexity afforded by the Suga model enables a slight but noticeable improvement for forced convection and early-onset mixed convection (i.e. Cases A and B). The same model is however late in predicting the re-laminarization and associated effects, and is thus in far poorer agreement with the reference results than its baseline model (LS).

6.4 Turbulence Quantities

Profiles of the turbulent kinetic energy (TKE) and its dissipation rate, ε, are shown in Figure 4(a) and (b), respectively. Once again, the predictions of the Suga model for forced convection and early-onset mixed convection (i.e. cases A and B) are significantly better than with LS. Indeed, the under-prediction of peak TKE by the LS model is well known and has been reported by a number of other researchers including Patel et al. [28] and Cotton and Kirwin [29]. Nevertheless, the re-laminarizing effect of buoyancy on turbulence is at least qualitatively captured by the LS model (Case C), as is the recovery of k for Case (D). In contrast, the results of the Suga model for Cases (C) and (D) are severely over- and under-predicted, respectively.

A similar trend can also be seen for the dissipation rate, ε in Figure 4(b). Although no profile was reported for ε by You et al., none of the profiles shown in Figure 4(b) are expected to be in good agreement with the DNS data especially near the wall due to highly approximate nature of the ε-equation [30]. The differences between the predictions of LS and Suga models seen in Figure 4(b) are partly associated with different definitions of the 'E-term' in the ε-transport equations of the models (compared in Table 2). This point will be discussed further in Section 6.6.4.

The Reynolds shear stress profiles are shown in Figure 4(c). Cases (A) and (B) are seen to have similar shear stress profiles, in that they are positive and peak in the region $y^+ \approx$ 20-30. In both cases (where forced convection is dominant), the predictions of the Suga model are in better agreement with the data than the LS model, as one might expect. For Case (C) it is observed that the DNS data indicate a laminarization of the flow, and a change in sign of the Reynolds stress in the core region. This reduction in stress levels is captured only by the LS model, which as discussed further on, predicts almost complete laminarization of the near-wall flow. In contrast, the Suga model is completely insensitive to the laminarization effects at

these conditions. The LS model captures the general trend of the data for Case (D), but fails to resolve the detail of the near-wall stress distribution, while the Suga model significantly under-predicts the magnitude of the shear stress, especially in the core region.

The turbulent viscosity ratio (TVR) is compared in Figure 5(a), where the impact of the above differences becomes more relevant, especially for Cases (C) and (D). In the LS model, the magnitude of the reduction in TVR from Cases (B) to (C) is predicted correctly; i.e. the magnitude of the turbulent viscosity reduces by increasing the buoyancy influence, until a complete laminarization occurs (Case C). With further increase of buoyancy influence, the region of zero TVR reduces which indicates that some of turbulence recovery is occurring (Case D). Comparing the two sets of profiles in Figure 5(a) suggests that the failure of the Suga model may be linked to the way the turbulent viscosity is permitted to respond to the increase of buoyancy influence. The reduction of TVR with respect to buoyancy influence is severely under-predicted by the Suga model. This under-prediction is consistent with the under-prediction of the heat transfer impairment observed in Figure 1.

Profiles of the damping function, f_μ, are given in Figure 5(b). Although the definition of f_μ in the Suga model is slightly different from that used in the LS model (compared in Table 2), the profiles for Cases (A) and (B) are somewhat similar. The profiles for Cases (C) and (D), however, are very different from those returned by the LS model, mainly due to differences in the distribution of Re_t which itself is proportional to k^2/ε. It is worth noting that even in non-linear eddy-viscosity models such as the Suga model, a Reynolds-number dependent damping term (i.e. f_μ) is required for near-wall flows, but its influence is considerably less than that used in linear EVMs, since a substantial amount of the near-wall strain-related damping is now provided by the functional form of C_μ [15] (this point is discussed further in Sections 6.6.1 and 6.6.3).

6.5 Budgets of the Turbulent Kinetic Energy

While examining the turbulent kinetic energy, or the rate of its dissipation is instructive, it is difficult to identify the source of a modelling problem by this process alone. Therefore, in order to see the influence of small change to terms in a model, we here examine the individual contribution of each term required for a balance of the modelling equations set out above; i.e. the budget of the transport equations. The budgets of the TKE for the forced convection and laminarization cases (i.e. Cases A and C) are plotted for both the Suga and LS models and are shown in Figure 6. Note that positive values indicate a local gain in TKE while negative values indicate a loss.

Figure 6 (a) shows the balance of terms in the k-equation, calculated for a fully-developed forced convection (Case A) using the Suga and LS models. Similar trends are predicted by both models, even though the LS model indicates slightly lower values. It is seen that the budgets returned by both models are largely dominated by the production and dissipation, except in the near-wall region. Very near to the wall,

the dissipation is balanced with the viscous diffusion and the maximum production and dissipation of k, occur at $y^+ \approx 12$. Also note that the viscous and turbulent diffusions change sign at approximately $y^+ \approx 10$ and $y^+ \approx 13$, respectively. The same is plotted for Case (C) in Figure 6(b), where the LS model returns a dramatically different balance from that of forced convection. As expected, in the results of the LS model, it can be seen that the values are much smaller than those of forced convection (with nearly two orders of magnitude) which are the indicators of the laminarization. In this case all the elements of the k-budget are equal to zero up to $y^+ \approx 20$. The production of k remains zero at the position where the maximum velocity occurs (i.e. $y^+ \approx 40$). Unlike Case (A), however, in the core region the production is balanced with the diffusion and dissipation terms. Contrary to this, the Suga model remains relatively insensitive to the laminarization and thus is unable to predict the expected drop in turbulence.

6.6 Further Modelling Refinements

6.6.1 Numerical Instability Issues

During the course of the present study, significant numerical instability issues were encountered with the Suga model, particularly for higher heat loading values (i.e. higher values of *Bo*). In fact, similar problems were found when simulating the same test case using the commercial code, STAR-CD (reported in [11]). Another example of these numerical issues was reported by Yakinthos et al. [31] for the simulation of a 90° rectangular duct. An attempt to resolve these issues was made by the original authors and their colleagues, including the work by Cooper [32], Raisee [33] and Craft et al. [34]. The investigations of Raisee [33] on ribbed passages identified the dependence of C_μ on the strain rate as the source of some of these problems. A subsequent investigation by Cooper [32] for an abrupt pipe expansion case indicated that the heat transfer over-prediction of the Suga model was, at least in part, due to the fact that C_μ exceeded its equilibrium value in regions of low near-wall strain rates, and hence, proposed to limit the maximum value of C_μ with some success. However, the numerical instability of the Suga model has not been investigated previously for mixed convection flows, where severe numerical issues have repeatedly been reported [11-13].

In light of the above findings, and motivated to further investigate the instability issues of the Suga model, the distributions of C_μ and non-dimensional strain rate, $\tilde{S}$, were examined, as plotted in Figure 7(a) and (b). Of most interest are the results associated with the recovery case i.e. Case (D), which has been identified as the most numerically unstable case. The C_μ profile in for Case (D) exhibits a complex behaviour, quite different to the other cases. Observed high levels of strain rate variations in the near-wall region ($y^+ < 5$) in Figure 7(b) are associated with a sharp reduction in C_μ; this is a coupled effect, likely to be linked to the numerical instability in question. Further away from the wall, in the region of $40 < y^+ < 60$, C_μ rises suddenly, which corresponds to a region of low strain rate (corresponding to the maximum of the velocity profile in Figure 3b). In fact, at $y^+ \approx 45$, the model predicts zero strain rate, which in turn leads to

a brief discontinuity in the C_μ distribution. As for the majority of low-Reynolds number EVMs, a damping function appears in the expression of turbulent viscosity, and is usually denoted as f_μ. Similar to the LS model, the Suga model employs a Re_t-dependent damping function, albeit with a different form. The overall damping of the turbulent viscosity would be achieved through $f_\mu \times C_\mu$, which is plotted in Figure 7(c). Comparing the distributions in Figure 7(c) to those in Figure 7(a) reveals the significant impact of C_μ on the overall damping of the Suga model.

Finally, Figure 7(d) shows the distributions of E_ε for all four cases. For Cases (A)-(C), this source term is only significant within $5 < y^+ < 50$ and it peaks at $y^+ \approx 15$ which is consistent with the profiles of ε shown in Figure 4(c). The profile of E_ε for Case (D), however, exhibits a very different trend, which includes a number of minima and maxima (shown more clearly in the inset) due to strong strain rate gradients and inaccurate turbulent viscosity predictions within $40 < y^+ < 60$.

6.6.2 Constant C_μ

Based on the observations discussed above, the first step to find out the source of the numerical instability in the present simulations, would be to investigate the effects of changing the C_μ formulation in the Suga model. In order to do so, in common with the majority of the two-equation EVMs, a constant value of $C_\mu = 0.09$ was used in this part of the study to replace the 'strain-sensitive' C_μ formulation in the original Suga model (see Table 2).

The calculations are repeated for all four thermal-hydraulic cases and initially it is found that setting C_μ to a constant value significantly improves the convergence and the numerical instabilities of the Suga model. However, from the mean flow and temperature profiles shown in Figure 8(a) and (b), it is evident that the Suga model with a constant C_μ, completely loses its sensitivity to the laminarization effects and returns profiles that are entirely turbulent for all four thermal-hydraulic regimes. The inaccuracy of the modified Suga model is further evident from the severe over-predictions of the TKE and Reynolds shear stress in Figure 8(c) and (d), compared to the DNS data and even the original Suga model. The failure of the modified Suga model seen in Figure 8 is mainly due to insufficient overall damping of the turbulent viscosity (represented by $f_\mu \times C_\mu$) in the near wall region, as seen in Figure 8(e).

As was alluded to earlier, in the original Suga model, a substantial amount of the near-wall strain-related damping is provided by the strain-sensitive C_μ function. Therefore, adopting a constant value for C_μ would produce insufficient damping of the turbulent viscosity in the near-wall region. Therefore, the modified Suga model returns high levels of TVR for all four cases (Figure 8f), which is ultimately responsible for returning poor mean flow and temperature profiles (Figure 8a and b).

6.6.3 New C_μ Formulation

As discussed in the previous sections, it is evident that the numerical instability issues of the Suga model in mixed convection flows are associated with the definition of C_μ. It was also found that using a constant value for C_μ has unfavourable effects on the performance of the model. Therefore, it is desirable to search for an alternative strain-sensitive definition for C_μ, which would ideally improve both the accuracy and the stability of the Suga model.

Following the work of Craft et al. [34] for a sudden pipe expansion and an impinging jet, in this paper we propose to use the following alternative expression for C_μ:

$$C_\mu = \min\left(0.09, \frac{1.2}{1+3.5\eta+f_{RS}}\right) \tag{8}$$

where

$$f_{RS} = 0.235\left(\max\left(0,\eta-3.333\right)\right)^2 \exp\left(-\frac{\mathrm{Re}_t}{400}\right) \tag{9}$$

$$\eta = \max\left(\widetilde{S},\widetilde{\Omega}\right) \tag{10}$$

This definition for C_μ, which has never been tested for mixed convection flows, is likely to reduce the sensitivity of C_μ to the strain rate in the regions further away from the wall (and potentially removes the need for smoothing C_μ). In addition, it limits the maximum value of C_μ in regions of low strain rate, hence, resolving the problem seen in Figure 7(a), above.

The results of using the above C_μ definition are shown in Figure 9. In Figure 9(a) and (b) it is evident that the mean flow and temperature profiles are only marginally affected by the new C_μ expression. However, the TKE and Reynolds shear stress profiles (Figure 9c and d) are affected to a greater extent; they are both indicated to be slightly higher as a consequence of a similar rise in levels of C_μ itself (Figure 9e). The new C_μ formulation also limits the maximum value of C_μ in regions of low strain rate; $y^+ > 65$ for Cases (A)-(C) and $40<y^+<50$ for Case (D). The low strain rate region (i.e. approximately $\widetilde{S}<5$) in Case (D) corresponds to the peak region of the velocity profile.

Furthermore, as can be seen in Figure 9(f), for Cases (A)-(C), the new C_μ expression results in slightly higher levels of TVR in the near-wall regions. However, due to a 'limiter' in Eqn. (8), the new C_μ expression returns lower μ_t/μ in the core region ($y^+ > 80$), a behaviour which is somewhat similar to that of the LS model (see Figure 5a).

It is important to highlight that, whilst no significant improvement was achieved by using the new C_μ expression, the numerical stability of the Suga model improved remarkably. With the original Suga model, the present flow domain would not run beyond a distance of 50*D* (see Section 3), despite many attempts to fine-tune the numerics. However, with the new C_μ expression, convergence was obtained for a flow domain

extended up to 500D. This finding confirms that the dependence of C_μ on the strain rate is undoubtedly the main source of numerical instability in the original Suga model. This finding provides a new opportunity for the turbulence modelling community to test alternative strain-sensitive C_μ formulations, similar to the one test in the present work, with an aim of improving the accuracy and stability of this popular NLEVM.

6.6.4 The Effects of E-term

In the present work, each of the four differences between the two models (summarised in Table 2), was tested systematically in order to isolate the root cause of the modelling failure in the laminarization case (i.e. Case C). The outcome of this trial suggested that the E-term (E_ε) in the original Suga model might be a source of inaccuracy in capturing the laminarization effects. While the LS model uses a similar near-wall source term, the expression of E_ε in the original Suga model was designed to be less dependent on the Reynolds number. To further investigate this point, the E-term in the original Suga model was replaced with that of the LS model and the simulations were repeated for all four thermal-hydraulic regimes given in Table 1 and the results are compared in Figure 10.

The mean flow and temperature profiles shown in Figure 10(a) and (b) indicate that the modified Suga model returns higher velocity magnitude for Cases (A)-(C) and higher temperatures for all cases, in the core region. It can also be seen that compared to the original model, the modified Suga model is generally in poorer agreement with the DNS data in all four cases. However, it is important to highlight that the E-term substitution has re-introduced a sensitivity between Cases (A)-(C), when compared to the original form of the Suga model. This sensitivity has more pronounced effects on the TKE and Reynolds shear stress profiles shown in Figure 10(c) and (d), where the differences between each thermal-hydraulic case is more significant compared to the original model. This suggests that changing the E-term would enable the Suga model to become more sensitive to the heat loading (i.e. the type of thermal-hydraulic regime), which for example leads to better predictions for Case (C) in Figure 10(c) and (d).

Figure 10(e) compares the distributions of E_ε for both the modified and original Suga models. Consistent with the TKE profiles, the modified Suga model returns significantly lower values, with the highest and lowest differences found for Cases (C) and (D), respectively.

The severe under-predictions of the turbulent kinetic energy in Figure 10(c), has resulted in the modified Suga model returning lower μ_t/μ in Figure 10(f) for both near-wall and core regions compared to the original Suga model, in spite of both models having similar profiles. It is also noted that the largest discrepancy between the two models can be found in Case (C). Furthermore, in Figure 10(f) it can be seen that for Cases (A)-(C), the TVR in both the original and modified Suga models tend to increase almost linearly with respect to the distance from the wall. This is mainly due to a quasi-linear overall damping of the turbulent viscosity in both models, represented by $f_\mu \times C_\mu$ (see Figure 7c), which is not directly influenced by the E-term definition. In contrast, the DNS data (and to a lesser extent the LS model - Figure 5a) show small

increase in the TVR beyond $y^+>60$ in all four cases. The discrepancy between the Suga model and the DNS data in predicting the turbulent viscosity, especially in the core region, indicates the potential of using alternative damping functions, which tend to limit the turbulent viscosity in the core region.

The results presented in this section, generally indicate that replacing the E-term of the original Suga model with that of the LS model leads to better predictions for the laminarization case (Case C), especially in predicting the level of turbulent kinetic energy. However, the performance for Cases (A) and (B) is deteriorated noticeably and, therefore, further work is required in order to refine and calibrate this term, so as to isolate this improvement to re-laminarization flows. This aspect is beyond the scope of the present study and is left for future work.

7 CONCLUSION

This paper investigates the mean flow and heat transfer in an ascending turbulent mixed convection pipe flow, which represents the coolant flow in the fuel elements of the UK fleet of Advanced Gas-cooled Reactors (AGRs). The aim of the present work was to carry out a meticulous assessment of the Suga non-linear eddy-viscosity model to identify the reasons for the failure of this commonly used turbulence model in mixed convection flows. The findings of this work would, amongst other areas, provide input to the turbulence modelling community for improving the performance and stability of this model for future applications, especially in the nuclear industry. As part of this study, the Suga model was implemented in an in-house CFD code, 'CONVERT', which, after successful verification and validation tests, was used to conduct all the computations presented here. Mean flow, heat transfer and turbulence quantities were obtained for four different thermal-hydraulic regimes (Table 1) and were compared against the predictions of the Launder-Sharma model and the DNS data.

The present study showed that indirect influence of the buoyancy force on the turbulence in an ascending vertical pipe flow is the dominant mechanism, which causes laminarization and impairment of heat transfer. It was also shown that for the laminarization and recovery regimes, inaccurate prediction of k^2/ε was responsible for returning inaccurate turbulent viscosity which in turn led to poor mean flow and heat transfer results.

Furthermore, the instability problems of the Suga model were also investigated and were shown to be related to the dependence of C_μ on the strain rate, which also contributed to the poor performance of this model in predicting the laminarization. Subsequently, an alternative expressions of C_μ proposed by Craft et al. [34] was tested which significantly improved the stability of the Suga model, while the mean flow profiles were marginally affected.

In an attempt to improve the performance of the Suga model, additional numerical tests were carried out in which the E-term in the original Suga model was replaced with that of the LS model. It was shown that the modified Suga model became more sensitive to the thermal-hydraulic regime. In particular, the substitute brought a significant improvement for the case of the flow re-laminarization. This work serves to demonstrate that the formulation of the E-term could play an important role in the future tuning of the Suga model, especially in heat transfer problems.

ACKNOWLEDGEMENTS

This work was partially funded by the UK Engineering and Physical Sciences Research Council 'Towards a Sustainable Energy Economy' (TSEC) programme 'Keeping the Nuclear Option Open' (KNOO). The authors are pleased to acknowledge the contribution of their colleagues in the School of Mechanical, Aerospace and Civil Engineering (MACE) at the University of Manchester, especially Dr. M.A. Cotton and Professor D. Laurence.

REFERENCES

1. W. P. Jones, and B. E. Launder. The prediction of laminarization with a two-equation model of turbulence, *Int. J. Heat Mass Transfer*, Vol. 15, pp. 301-314, 1972.

2. A. Keshmiri. Three-dimensional simulation of a simplified advanced gas-cooled reactor fuel elements, *Nuclear Eng. Design*, Vol. 241, pp. 4122-4135, 2011.

3. J. D. Jackson, M. A. Cotton, and B. P. Axcell. Studies of mixed convection in vertical tubes, *Int. J. Heat Fluid Flow*, Vol. 10, pp. 2-15, 1989.

4. J. D. Jackson. Studies of buoyancy-influenced turbulent flow and heat transfer in vertical passages, *Keynote lecture, 13th Int. Heat Transfer Conference, 'IHTC13'*, Sydney, Australia, 2006.

5. A. M. Abdelmeguid, and D. B. Spalding. Turbulent flow and heat transfer in pipes with buoyancy effects, *J. Fluid Mech.*, Vol. 94, pp. 383-400, 1979.

6. H. Tanaka, S. Maruyama, and S. Hatano. Combined forced and natural convection heat transfer for upward flow in a uniformly heated vertical pipe, *Int. J. Heat Mass Transfer*, Vol. 30, pp. 165-174, 1987.

7. M. A. Cotton, and J. D. Jackson. Vertical tube air flows in the turbulent mixed convection regime calculated using a low-Reynolds-number k-ε model, *Int. J. Heat Mass Transfer*, Vol. 33, pp. 275-286, 1990.

8. D. P. Mikielewicz, A. M. Shehata, J. D. Jackson, and D. M. McEligot. Temperature, velocity and mean turbulence structure in strongly heated internal gas flows Comparison of numerical predictions with data, *Int. J. Heat Mass Transfer,* Vol. 45, pp. 4333-4352, 2002.

9. A. H. Richards, R. E. Spall, and D. M. McEligot. An assessment of turbulence models for strongly-heated internal gas flows, *Proc. 15th IASTED Int. Conf. on Modeling and Simulation*, Marina Del Rey, California, USA, 2004.

10. W. S. Kim, S. He, and J. D. Jackson. Assessment by comparison with DNS data of turbulence models used in simulations of mixed convection, *Int. J. Heat Mass Transfer,* Vol. 51, pp. 1293-1312, 2008.

11. A. Keshmiri, M. Cotton, Y. Addad, and D. Laurence. Turbulence Models and Large Eddy Simulations Applied to Ascending Mixed Convection Flows, *Flow, Turbulence and Combustion,* Vol. 89, No. 3, pp. 407-434, 2012.

12. A. Keshmiri. Effects of various physical and numerical parameters on heat transfer in vertical passages at relatively low heat loading, *ASME Journal of Heat Transfer,* Vol. 133, pp. 092502-1, 2011.

13. A. Keshmiri, J. C. Uribe, and N. Shokri. Benchmarking of Three Different CFD Codes in Simulating Natural, Forced and Mixed Convection Flows, *J. Numerical Heat Transfer; Part A: Applications,* Vol. 67, pp. 1324-1351, 2015.

14. F. R. Menter. Two-equation eddy-viscosity turbulence models for engineering applications, *AIAA J.*, Vol. 32, pp. 1598-1605, 1994.

15. T. J. Craft, B. E. Launder, and K. Suga. Development and application of a cubic eddy-viscosity model of turbulence, *Int. J. Heat Fluid Flow*, Vol. 17, pp. 108-115, 1996.

16. J. Mahaffy, B. Chung, F. Dubois, F. Ducros, E. Graffard, M. Heitsch, M. Henriksson, E. Komen, F. Moretti, and T. Morii. Best practice guidelines for the use of CFD in nuclear reactor safety applications, *NEA/CSNI*, 2007.

17. B. E. Launder, and B. I. Sharma. Application of the energy dissipation model of turbulence to the calculation of flow near a spinning disc, *Lett. Heat Mass Transfer*, Vol. 1, pp. 131-138, 1974.

18. J. You, J. Y. Yoo, and H. Choi. Direct numerical simulation of heated vertical air flows in fully developed turbulent mixed convection, *Int. J. Heat Mass Transfer*, Vol. 46, pp. 1613-1627, 2003.

19. M. A. Cotton. Theoretical studies of mixed convection in vertical tubes, *Dept. of Engineering*. Ph.D. Thesis, University of Manchester, UK, 1987.

20. M. A. Leschziner. An introduction and guide to the computer code PASSABLE, *Dept. of Mech. Engineering, UMIST (now University of Manchester)*, 1982.

21. K. Suga. Development and application of a non-linear eddy viscosity model sensitized to stress and strain invariants, *Dept. of Mechanical Engineering*. Ph.D. Thesis, UMIST (now University of Manchester), UK, 1995.

22. J. Kim, P. Moin, and R. Moser. Turbulence statistics in fully developed channel flow at low Reynolds number, *J. Fluid Mechanics Digital Archive*, Vol. 177, pp. 133-166, 1987.

23. A. Keshmiri. Thermal-hydraulic analysis of Gas-cooled reactor core flows, *School of Mechanical, Aerospace and Civil Engineering*. Ph.D. Thesis, University of Manchester, UK, 2010.

24. C. R. Yap. Turbulent heat and momentum transfer in recirculating and impinging flows, *Dept. of Mech. Engineering, Faculty of Technology*. Ph.D. Thesis, UMIST (now University of Manchester), UK, 1987.

25. A. Steiner. On the reverse transition of a turbulent flow under the action of buoyancy forces, *J. Fluid Mech.*, Vol. 47, pp. 503-512, 1971.

26. A. D. Carr, M. A. Connor, and H. O. Buhr. Velocity, temperature and turbulence measurements in air for pipe flow with combined free and forced convection, *J. Heat Transfer*, Vol. 95, Trans. ASME C, pp. 445-452, 1973.

27. Y. Parlatan, N. E. Todreas, and M. J. Driscoll. Buoyancy and property variation effects in turbulent mixed convection of water in vertical tubes, *J. Heat Transfer*, Vol. 118, pp. 381-387, 1996.

28. V. C. Patel, W. Rodi, and G. Scheuerer. Turbulence models for near-wall and low Reynolds number flows: A Review, *AIAA J.*, Vol. 23, pp. 1308-1319, 1985.

29. M. A. Cotton, and P. J. Kirwin. A variant of the low-Reynolds-number two-equation turbulence model applied to variable property mixed convection flows, *Int. J. Heat Fluid Flow*, Vol. 16, pp. 486-492, 1995.

30. M. A. Cotton, and J. O. Ismael. A strain parameter turbulence model and its application to homogeneous and thin shear flows, *Int. J. Heat Fluid Flow*, Vol. 19, pp. 326-337, 1998.

31. K. Yakinthos, Z. Vlahostergios, and A. Goulas. Modeling the flow in a 90° rectangular duct using one Reynolds-stress and two eddy-viscosity models, *Int. J. Heat Fluid Flow*, Vol. 29, No. 1, pp. 35-47, 2008.

32. D. Cooper. Computation of momentum and heat transfer in a separated flow, using low-Reynolds-number linear and non-linear k-ε models, *Dept. of Mechanical Engineering*. M. Res. Dissertation, UMIST (now University of Manchester), UK, 1997.

33. M. Raisee. Computation of flow and heat transfer through two- and three-dimensional rib-roughened passages, *Dept. of Mechanical Engineering.* Ph.D. Thesis, UMIST (now University of Manchester), UK, 1999.

34. T. J. Craft, H. Iacovides, and J. H. Yoon. Progress in the use of non-linear two-equation models in the computation of convective heat transfer in impinging and separated flows, *Flow, Turbulence and Combustion,* Vol. 63, pp. 59-80, 1999.

TABLES

Case	Gr/Re^2	Bo	Thermal-Hydraulic Regime
A	0	0	Forced convection
B	0.252	0.13	Early-onset mixed convection
C	0.348	0.18	Laminarization
D	0.964	0.50	Recovery

Table 1. DNS cases of You et al. [18].

Variable	LS k-ε model	Suga k-ε model
$\overline{u_i u_j}$	$-\nu_t S_{ij} + (2/3)k\delta_{ij}$	$(2/3)k\delta_{ij} - \nu_t S_{ij} + c_1\nu_t\frac{k}{\varepsilon}(S_{ik}S_{jk} - 1/3 S_{kl}S_{kl}\delta_{ij})$ $+c_2\nu_t\frac{k}{\varepsilon}(W_{ik}S_{kj} + W_{jk}S_{ki})$ $+c_3\nu_t\frac{k}{\varepsilon}(W_{ik}W_{jk} + 1/3 W_{lk}W_{lk}\delta_{ij})$ $+c_4\nu_t\frac{k^2}{\varepsilon^2}(S_{ki}W_{lj} + S_{kj}W_{li})S_{kl}$ $+c_5\nu_t\frac{k^2}{\varepsilon^2}(W_{il}S_{mj} + S_{il}W_{mj} - 2/3 S_{\ln}W_{mn}\delta_{ij})W_{lm}$ $+c_6\nu_t\frac{k^2}{\varepsilon^2}S_{ij}S_{kl}S_{kl} + c_7\nu_t\frac{k^2}{\varepsilon^2}S_{ij}W_{kl}W_{kl}$
C_μ	0.09	$\frac{0.3}{1+0.35\left(\max(\tilde{S},\tilde{\Omega})\right)^{1.5}}\times$ $\left(1-\exp\left[\frac{-0.36}{\exp\left(-0.75\max(\tilde{S},\tilde{\Omega})\right)}\right]\right)$
f_μ	$\exp\left[-3.4/\left(1+\frac{Re_t}{50}\right)^2\right]$	$1 - \exp\left[-(Re_t/90)^{1/2} - (Re_t/400)^2\right]$
E_ε	$2\nu\nu_t\left(\frac{\partial^2 U_i}{\partial x_j \partial x_k}\right)^2$	$\begin{cases} 0.0022\frac{\tilde{S}\nu_t k^2}{\tilde{\varepsilon}}\left(\frac{\partial^2 U_i}{\partial x_j \partial x_k}\right)^2 & \text{for } Re_t \le 250 \\ 0 & \text{for } Re_t > 250 \end{cases}$

Table 2. Functions appearing in the LS and Suga turbulence models.

Constants	LS k-ε model	Suga k-ε model
σ_k	1.0	1.0
σ_ε	1.3	1.3
$C_{\varepsilon 1}$	1.44	1.44
$C_{\varepsilon 2}$	1.92	1.92

Table 3. Constants appearing in the LS and Suga models.

c_1	c_2	c_3	c_4	c_5	c_6	c_7
-0.1	0.1	0.26	-10 C_μ^2	0	-5 C_μ^2	5 C_μ^2

Table 4. Constants appearing in the Reynolds shear stress equation of the Suga model.

Models/Techniques	Nu_0	% diff.	c_{f0}	% diff.
DNS of You et al. [18]	18.3	–	9.28×10^{-3}	–
Launder-Sharma model	17.4	- 4.9	8.52×10^{-3}	- 8.2
Suga model	18.3	0	8.93×10^{-3}	- 3.8

Table 5. Results for fully-developed forced convection.

FIGURES CAPTIONS

Figure 1. Normalised Nusselt number distribution in ascending mixed convection flows.

Figure 2. Normalised friction coefficient distribution in ascending mixed convection flows.

Figure 3. Mean flow profiles obtained using the Suga and Launder-Sharma models.

Figure 4. Turbulence quantities from the Suga and LS models.

Figure 5. Turbulent viscosity ratio and damping function from the Suga and LS models.

Figure 6. Budgets of the turbulent kinetic energy obtained using the Suga and Launder-Sharma model; (a) Case A (Forced Convection) and (b) Case C (Laminarization).

Figure 7. Distribution of various low-Reynolds number functions in the Suga model.

Figure 8. The effects of setting C_μ =0.09 in the Suga model.

Figure 9. The effects of using a new C_μ expression in the Suga model.

Figure 10. The effects of replacing the E-term of the original Suga model with that of the LS model.

FIGURES

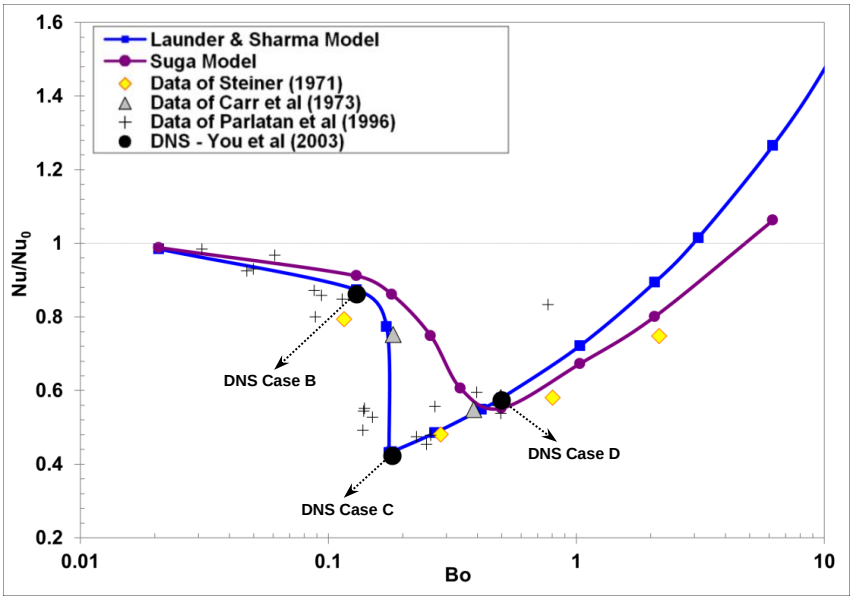

Figure 1. Normalised Nusselt number distribution in ascending mixed convection flows.

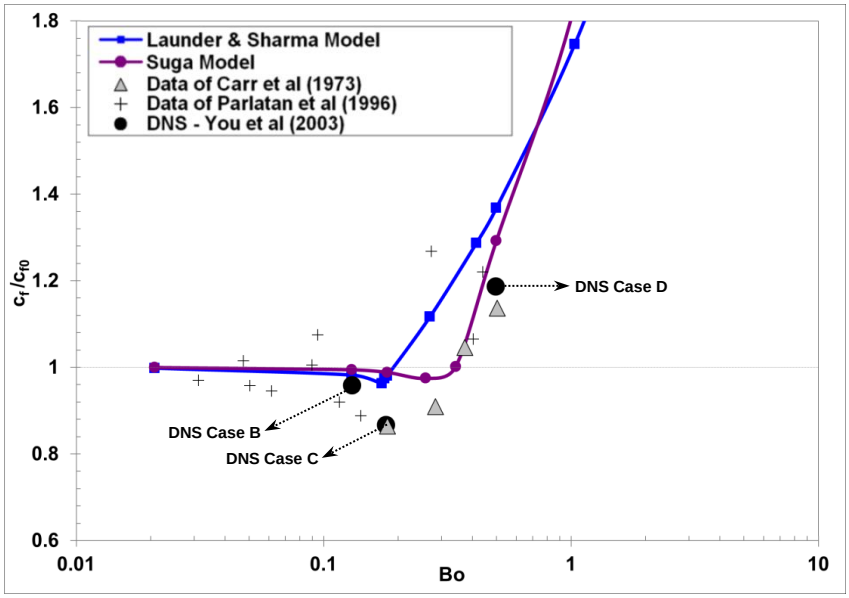

Figure 2. Normalised friction coefficient distribution in ascending mixed convection flows.

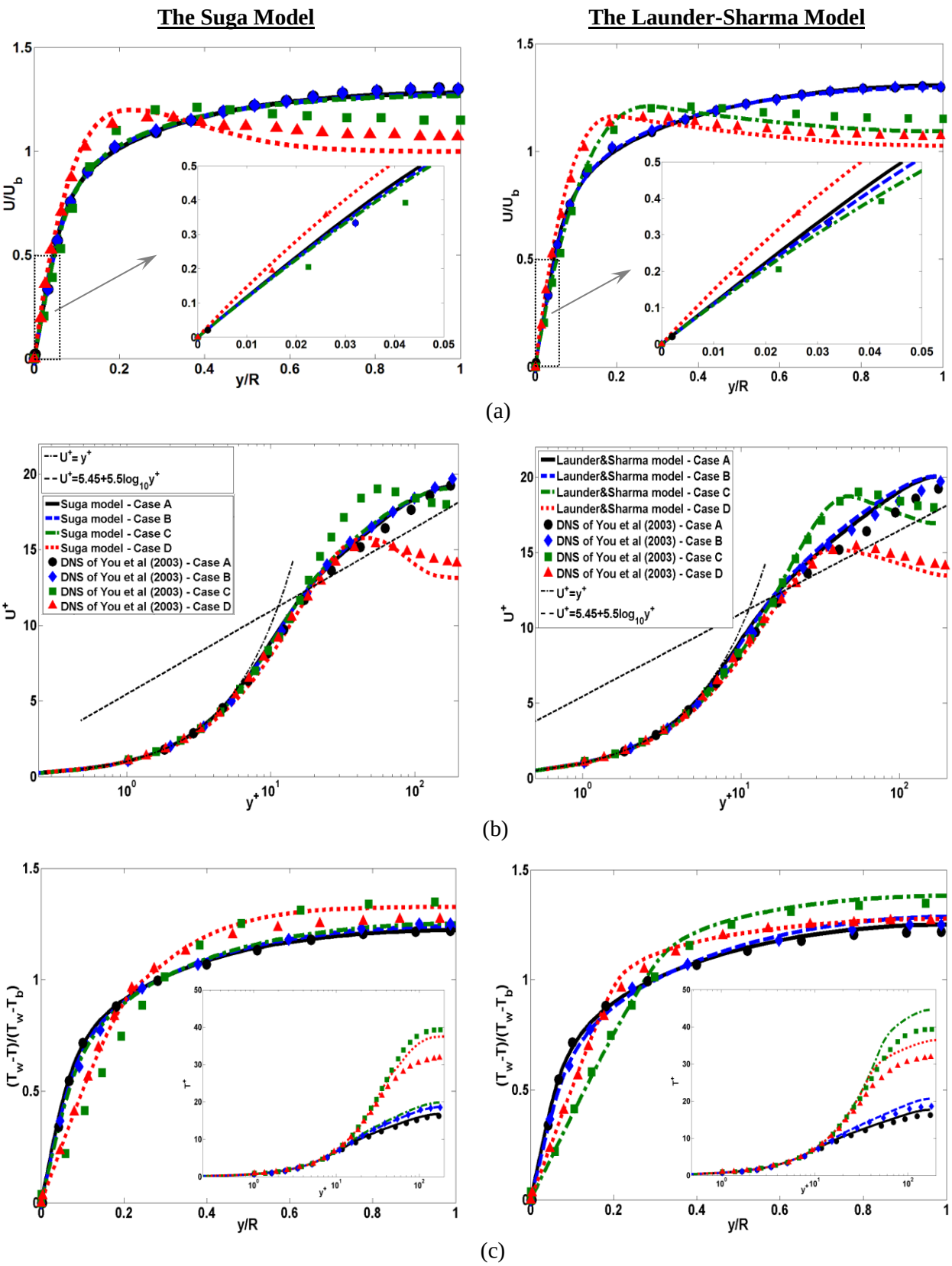

Figure 3. Mean flow profiles obtained using the Suga and Launder-Sharma models.

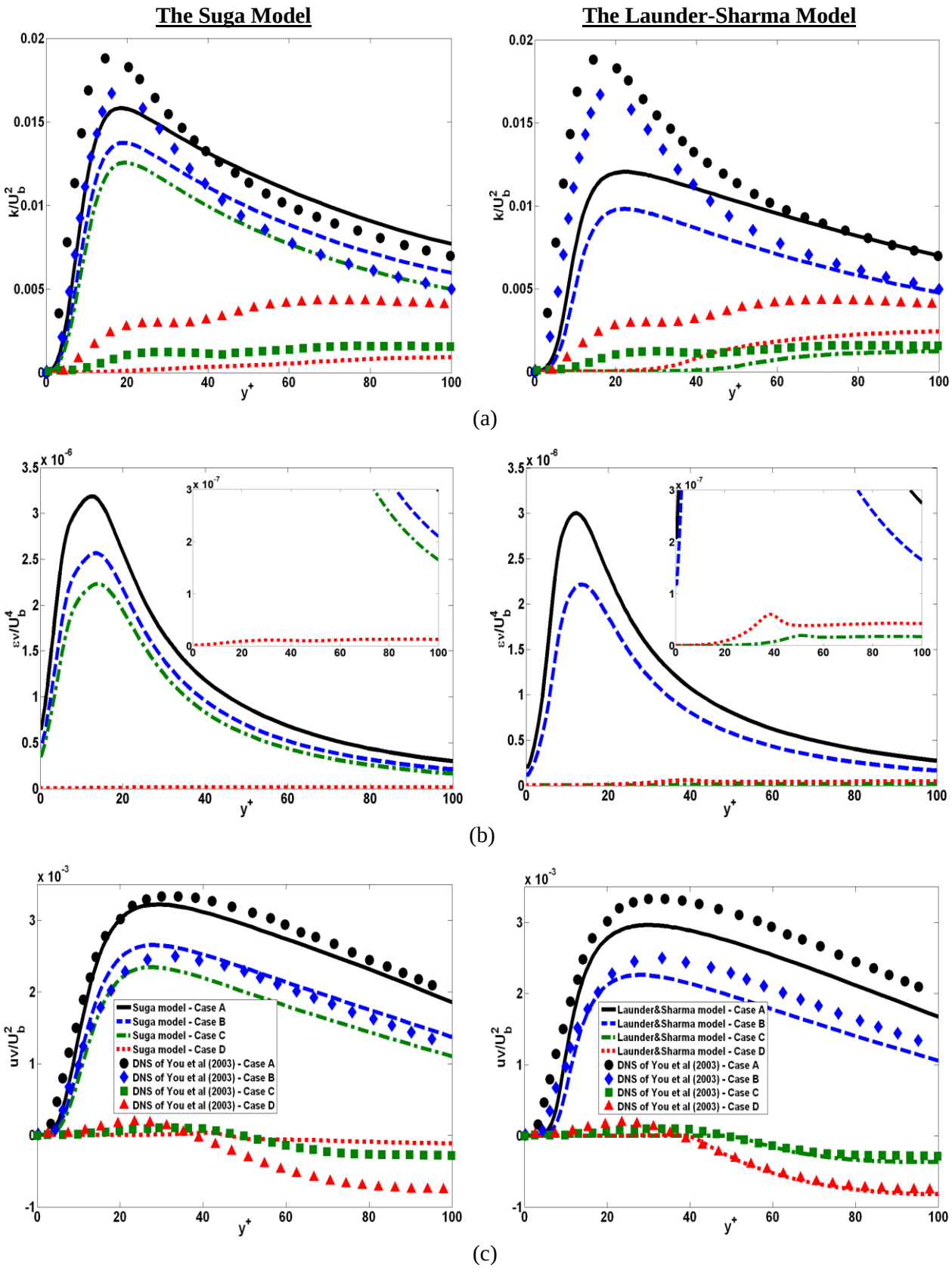

Figure 4. Turbulence quantities from the Suga and LS models.

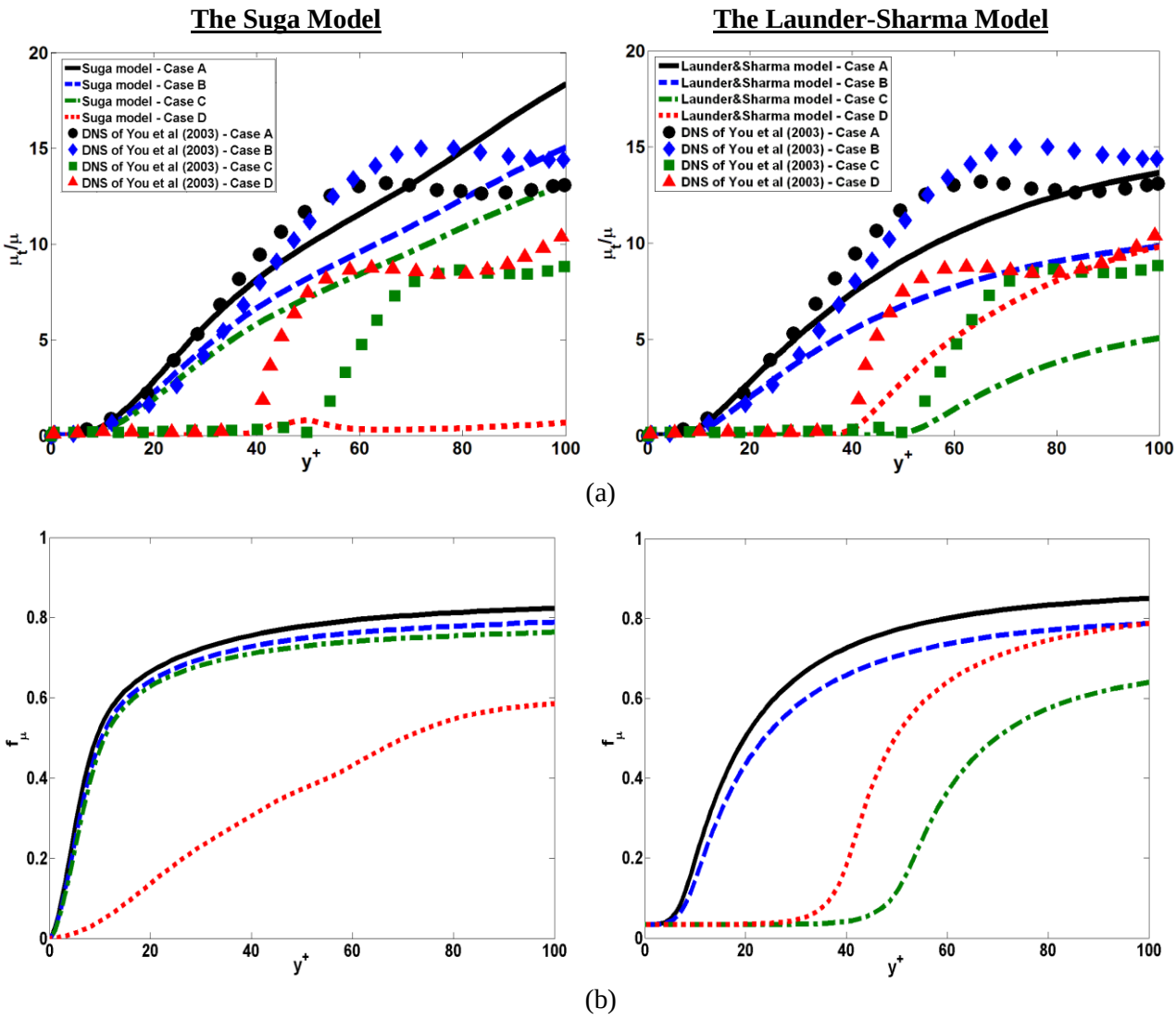

Figure 5. Turbulent viscosity ratio and damping function from the Suga and LS models.

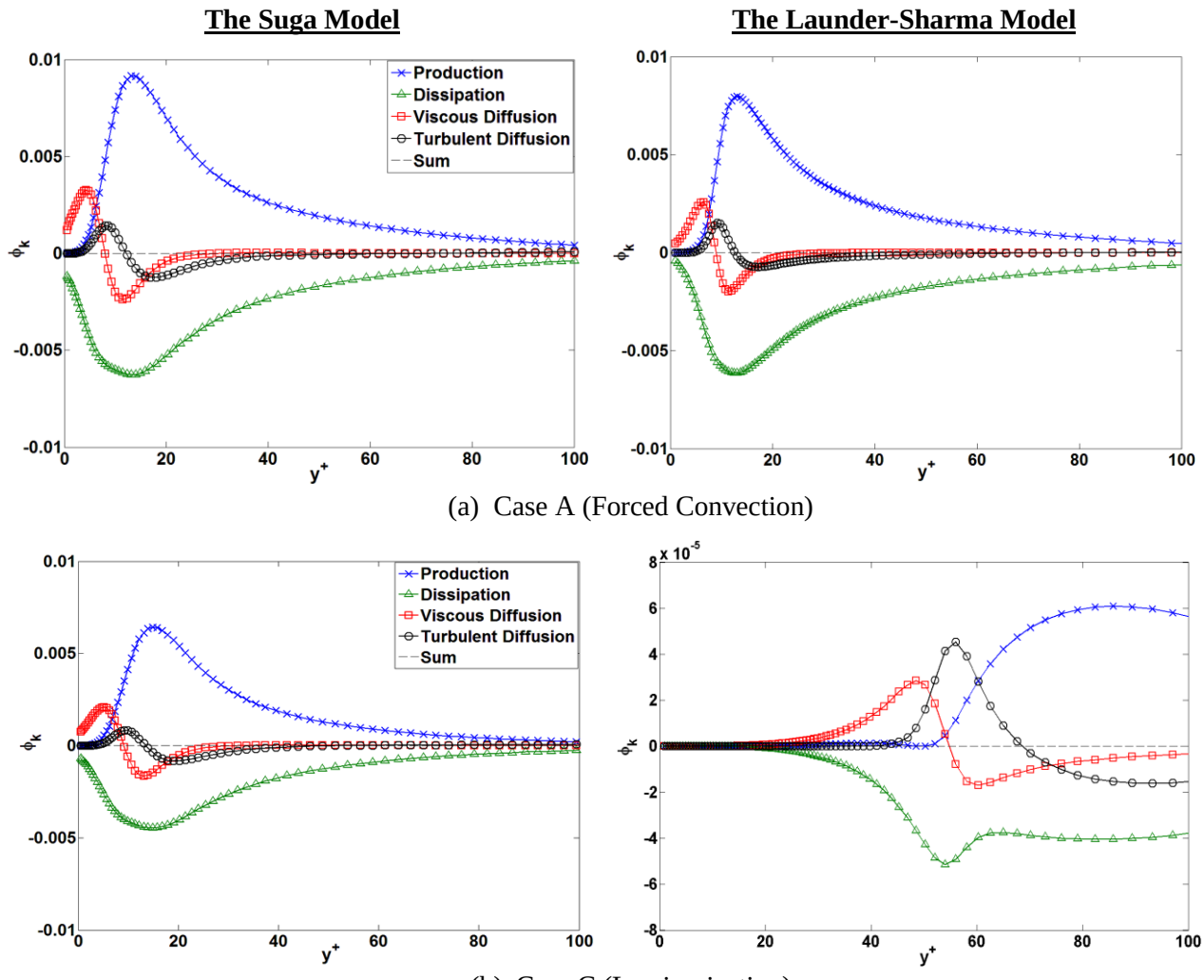

(a) Case A (Forced Convection)

(b) Case C (Laminarization)

Figure 6. Budgets of the turbulent kinetic energy obtained using the Suga and Launder-Sharma model; (a) Case A (Forced Convection) and (b) Case C (Laminarization).

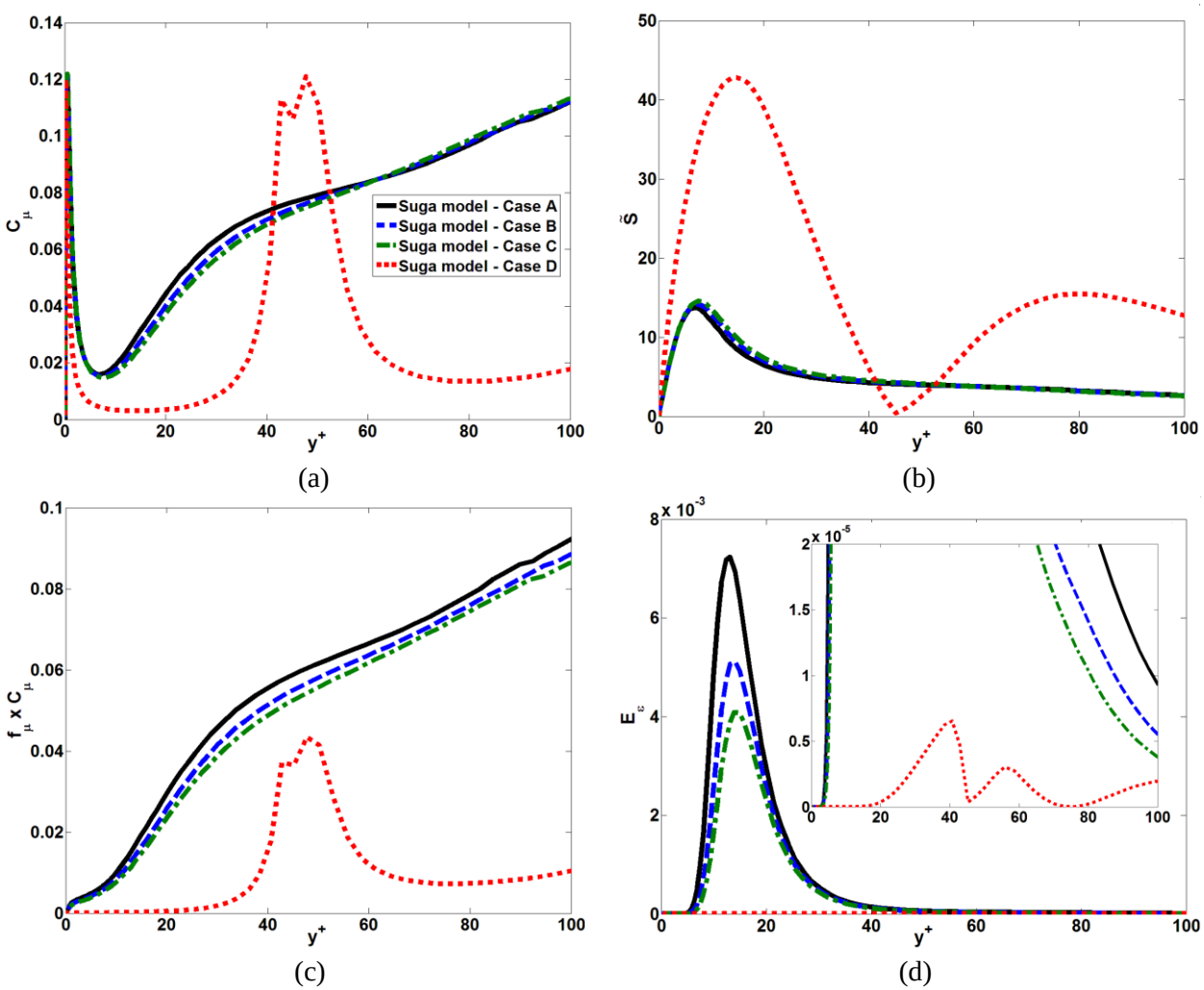

Figure 7. Distribution of various low-Reynolds number functions in the Suga model.

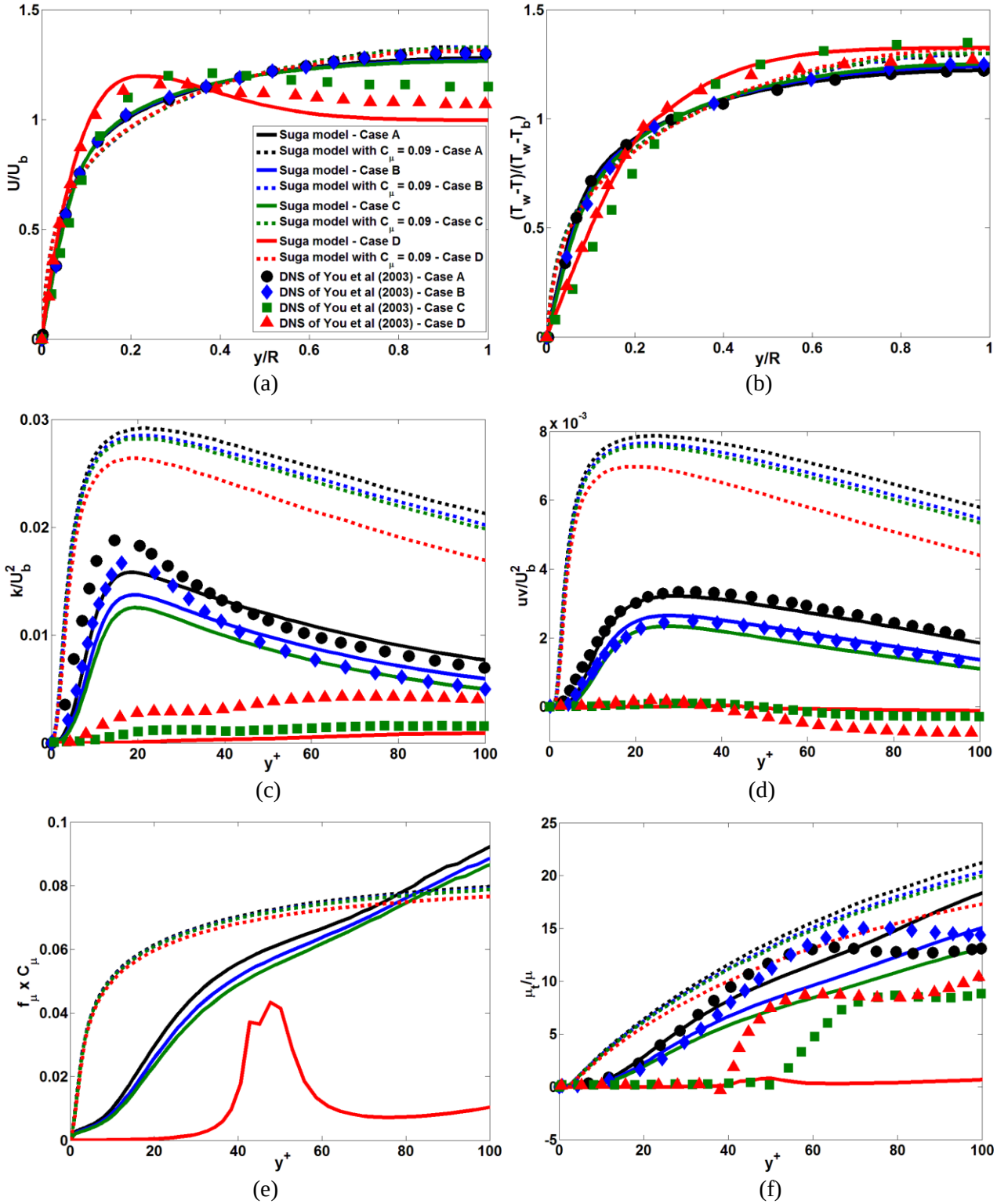

Figure 8. The effects of setting C_μ =0.09 in the Suga model.

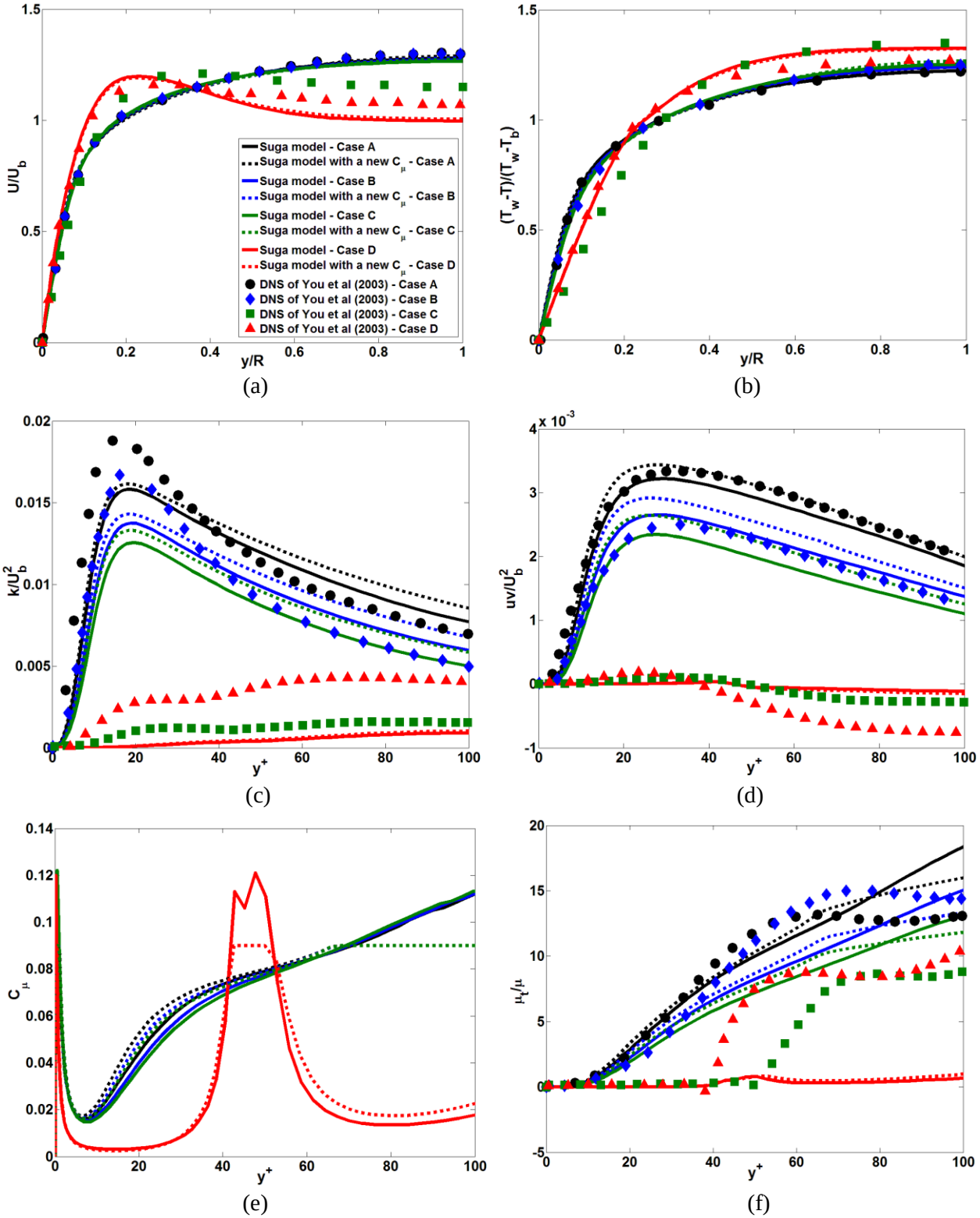

Figure 9. The effects of using a new C_μ expression in the Suga model.

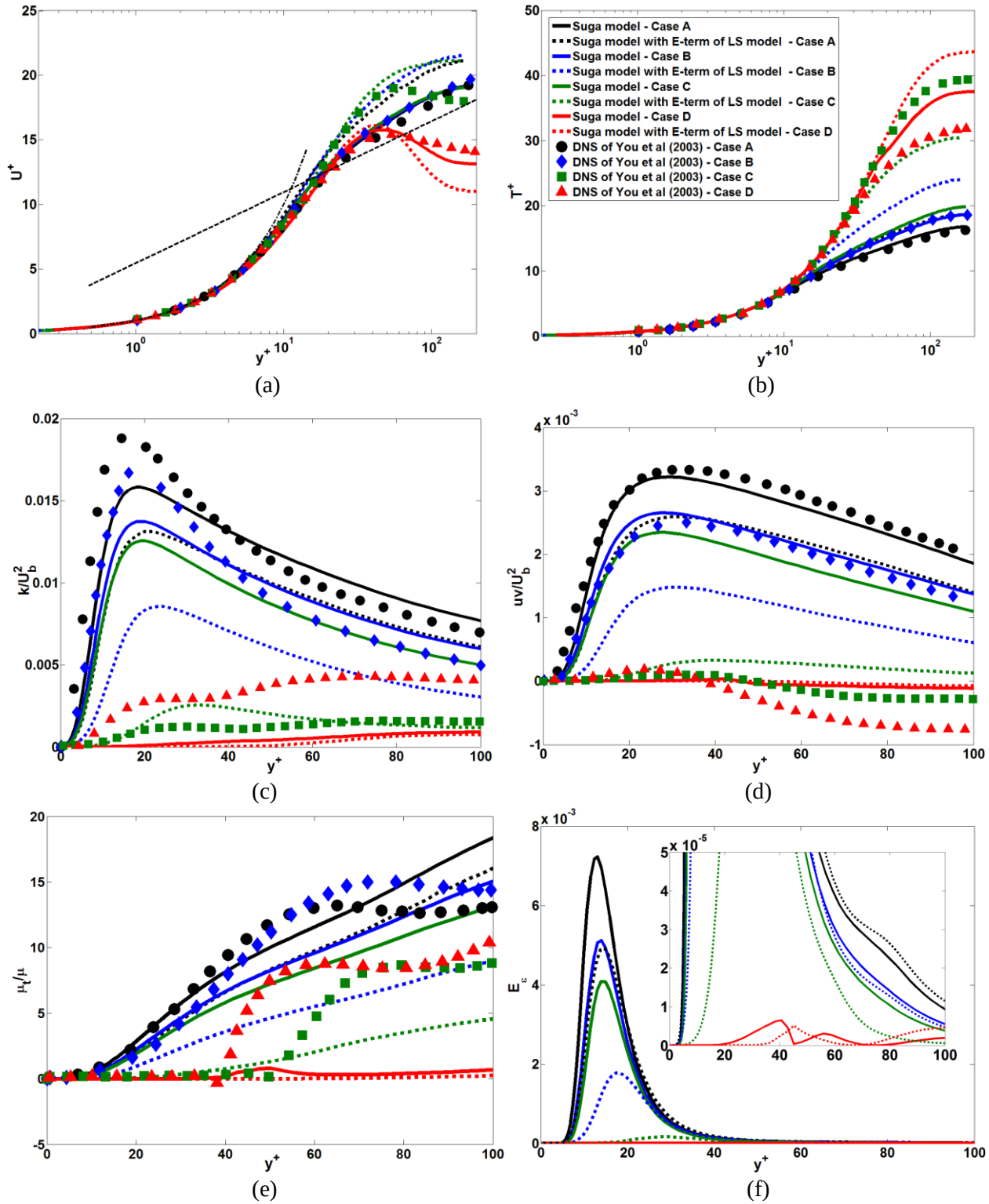

Figure 10. The effects of replacing the E-term of the original Suga model with that of the LS model.